Letter

Determination of the ^{8}B neutrino energy spectrum using trapped ions

B. Longfellow,[1] A. T. Gallant,[1] T. Y. Hirsh,[2] M. T. Burkey,[1] G. Savard,[3,4] N. D. Scielzo,[1] L. Varriano,[3,4] M. Brodeur,[5] D. P. Burdette,[3,5] J. A. Clark,[3] D. Lascar,[3,6] P. Mueller,[3] D. Ray,[3,7,*] K. S. Sharma,[7] A. A. Valverde,[3,7] G. L. Wilson,[8] and X. L. Yan[3]

[1]*Lawrence Livermore National Laboratory, Livermore, California 94550, USA*
[2]*Soreq Nuclear Research Center, Yavne 81800, Israel*
[3]*Physics Division, Argonne National Laboratory, Argonne, Illinois 60439, USA*
[4]*Department of Physics, University of Chicago, Chicago, Illinois 60637, USA*
[5]*Department of Physics and Astronomy, University of Notre Dame, Notre Dame, Indiana 46556, USA*
[6]*Department of Physics and Astronomy, Northwestern University, Evanston, Illinois 60208, USA*
[7]*Department of Physics and Astronomy, University of Manitoba, Winnipeg, Manitoba, Canada R3T 2N2*
[8]*Department of Physics and Astronomy, Louisiana State University, Baton Rouge, Louisiana 70803, USA*

(Received 3 September 2022; accepted 22 March 2023; published 31 March 2023)

The β^+ decay of ^{8}B provides the dominant source of solar neutrinos above 2 MeV. Consequently, experiments that detect neutrinos from the sun require an accurate determination of the ^{8}B neutrino energy spectrum. In this work, the β-decay Paul trap surrounded by double-sided silicon strip detectors was utilized to precisely measure the decay products of trapped ^{8}B ions. The results were used to determine the ^{8}Be final-state distribution and to reconstruct the neutrino energy spectrum. This measurement using trapped ions is the first of its kind and puts the neutrino energy spectrum on much firmer footing by discriminating between recently reported values for the maximum of the final-state distribution.

DOI: 10.1103/PhysRevC.107.L032801

The Homestake experiment reported a large deficit between observed and predicted solar neutrino fluxes measured through electron neutrino capture on ^{37}Cl [1]. This disparity, known as the solar neutrino problem, was explained by enhanced neutrino flavor oscillations in matter via the Mikheyev-Smirnov-Wolfenstein effect [2–4] through measurements sensitive to electron, muon, and tau neutrinos at the Sudbury Neutrino Observatory (SNO) and Super-Kamiokande [5–7]. In these measurements, the vast majority of detected neutrinos originated from the β^+ decay of ^{8}B, which dominates the solar neutrino flux above 2 MeV [8].

Today, with the increasing reach of experiments, the underlying nuclear data for the neutrino energy spectrum need to be determined to high precision. Since neutrino oscillations modify the neutrino energy spectrum shape, precise knowledge of the undistorted ^{8}B neutrino spectrum is vital for the interpretation of solar neutrino experiments (see, e.g., Refs. [9–13]) and can be utilized to place limits on dark matter in the sun's core [14,15]. In particular, it would benefit next-generation facilities including Hyper-Kamiokande, *SNO+*, DUNE, and JUNO, which aim to make nonstatistically limited measurements of the 1–3% day/night asymmetry in electron neutrino flux due to oscillations within the earth and of the *hep* neutrino flux that extends only slightly beyond the ^{8}B neutrinos in energy [16].

The undistorted ^{8}B neutrino spectrum has been deduced through measurements of the excitation energy spectrum of ^{8}Be, which immediately breaks into two α particles, following ^{8}B β^+ decay. This β decay predominately populates a broad state peaking at about 3 MeV in excitation energy, the maximum of which strongly impacts the corresponding neutrino spectrum. However, discrepant results have been obtained for this final-state distribution (FSD). Bahcall *et al.* showed that initial experiments yielded a spread of $\pm$80 keV for the FSD peak [17], prompting measurements aimed at greater precision. At Notre Dame, Ortiz *et al.* implanted ^{8}B into a thin carbon foil flanked by two silicon detectors and measured the FSD maximum as 2899(12) keV via $\alpha-\alpha$ coincidences [18]. However, energy loss uncertainties in Ref. [18] due to carbon buildup on targets were underestimated [19]. Next, Winter *et al.* implanted ^{8}B into a silicon detector at Argonne National Laboratory to directly measure the summed α energies and obtained a higher maximum at 2943(9) keV [20,21]. Using the single-α technique at Seattle and considering lepton recoil, Bhattacharya *et al.* obtained a consistent maximum of 2939(5) keV [22].

However, two recent experiments by the same collaboration at IGISOL [23] and KVI [24] using techniques similar to the Notre Dame and Argonne measurements have resulted in maxima lower than those in Refs. [21,22]. The IGISOL result reported by Kirsebom *et al.* was 2921(5) keV [23] while the KVI result reported by Roger *et al.* was 2925(6) keV

*Present address: Physics Department, McGill University, Montreal, Quebec, Canada H3A 2T8, and TRIUMF, Vancouver, British Columbia, Canada V6T 2A3.

[24], later updated to 2923 keV [25,26]. The IGISOL/KVI collaboration has argued that the FSD differences could be due to Ref. [21] not correctly accounting for the differing response of silicon detectors to α particles and ^{16}O ions and Ref. [22] overestimating their detector response's low-energy tail [27]. The disagreement between the sets of results has remained unresolved, impacting the precision with which the solar neutrino spectrum can be interpreted and motivating a new experimental approach for studying ^{8}B β^{+} decay to settle this issue.

Here, for the first time, we utilize ion-trapping techniques to determine the ^{8}Be FSD maximum from ^{8}B β^{+} decay. The results in this Letter discern between the Argonne/Seattle and IGISOL/KVI maxima and were used to calculate the ^{8}B neutrino spectrum. In ion traps, radioactive nuclei can be held nearly at rest in a small, localized volume. The decay products emerge essentially scattering-free. The measurement was performed with the β-decay Paul trap (BPT) [28] surrounded by double-sided silicon strip detectors (DSSDs). This setup was used in precision measurements of ^{8}Li β^{-} decay to place limits on tensor currents in the weak interaction [29–31]. The apparatus and surrounding detectors were characterized in great detail for these studies [30–32], which rely on the energy differences of coincident α particles. Here, the FSD is calculated using the sum of the α energies, circumventing uncertainties from unfolding single α spectra [17,22]. Furthermore, this setup avoids the β-summing issues of the direct implantation method [21,24] and energy loss uncertainties due to implanting ^{8}B in an external foil [18,23]. Remaining systematic effects, including the DSSD line shape and the ability to distinguish between α and β particles, were scrutinized and accounted for in detail.

The experiment was performed at the ATLAS facility at Argonne National Laboratory. The radioactive ^{8}B beam was produced via two-proton transfer on a ^{6}Li primary beam traversing a cryogenic ^{3}He gas target. The reaction products were focused into a gas catcher using a large solenoid and then extracted, cooled, bunched, and delivered [33] to the preparation gas-filled Penning trap [34]. The ^{8}B activity was distributed across a variety of molecules, peaking at $A = 42$ [likely ^{8}B(OH)$_2$]. The $A = 42$ beam was delivered to the BPT.

Surrounding the BPT were four $64 \times 64 \times 1$ mm^3 DSSDs. Both the front and back sides were segmented into 32 strips. The energy calibration was performed *in situ* using two ^{148}Gd and two ^{244}Cm spectroscopy-grade calibration sources, providing α energies at 3182.690(24) keV [35] and 5804.77(5) keV [36], respectively. The calibration accounted for detector deadlayers, nonionizing energy losses, the pulse-height defect, source angles relative to the trap center, and source thicknesses. To provide a low-energy calibration point, the β minimum ionizing spectra from ^{8}B β^{+} decay were matched to GEANT4 simulations benchmarked against cosmic-ray muon data [32]. The systematic uncertainties for the α energies were taken from Ref. [32] with the source thickness uncertainty neglected due to the new, spectroscopy-grade sources. The muon peak uncertainty [32] was adopted as the systematic uncertainty for the β peak. The calibration was performed following Ref. [31] with energy-dependent uncertainty evaluated through standard error propagation accounting for covariances.

The ^{8}Be FSD was determined using the energies of two coincident α particles striking opposite-facing DSSDs within a 1-μs time difference ("doubles"). Random coincidences with larger timing differences were utilized for background subtraction. Based on GEANT4 simulations of the α and β spectra, hits with energies between 200 and 700 keV were considered β particles, while hits with energies greater than 700 keV were considered α particles. To ensure ion cloud thermalization, events within 35 ms of the trap closing were discarded. Furthermore, only events with a doubles multiplicity of 1 were considered to avoid ambiguities in identifying correct $\alpha-\alpha$ pairs. Additional cuts include the two α energies being within 600 keV and the front minus back α-energy difference being within -80 to 140 keV, where the asymmetry incorporates the satellite peak from back-strip charge sharing. Back-strip energies were only used in data selection. The edge strips, which are most sensitive to incomplete charge collection, were excluded from analysis. Six, one, six, and four nonedge strips with poor energy resolution were also excluded for the top, bottom, left, and right DSSDs, respectively.

The doubles detection efficiency was determined from detailed simulations of the decay kinematics and the experimental setup. ^{8}B β^{+} decays were generated using the comprehensive Monte Carlo simulation described in Refs. [29,30] that includes radiative [37] and recoil-order corrections [38]. The ^{8}B ion cloud size was accounted for and found from imaging [28] to be Gaussian distributed, extending 1.17 mm radially and 3.14 mm axially at 1σ. The BPT geometry, with surrounding detectors and infrastructure, was imported to GEANT4. β particles from the decay generator were propagated through the BPT GEANT4 geometry to account for scattering and the DSSD response. For α particles, the detector line shape was applied separately. To do this, a model of the DSSD detector response was developed using the spectroscopy-grade ^{148}Gd and ^{244}Cm sources and a separate detector characterization measurement using an α beam. The model is similar to that of Ref. [39], consisting of a main Gaussian with a tail arising from nonionizing energy losses added to a smaller component that is the same Gaussian plus tail with an additional, longer exponential tail representing charge sharing and incomplete charge collection due to crystal lattice damage [40–42]. The effects of the interstrip gaps and aluminum strips were also included. Finally, the simulated data were passed through the same sortcode as the experimental data to apply identical cuts.

Figure 1 shows the efficiency-corrected FSD derived from the experimental doubles. The excitation energy $E_x = E_{\alpha 1} + E_{\alpha 2} - S_\alpha - E_R$, where $E_{\alpha 1,2}$ are the α-particle energies, $S_\alpha = 91.8$ keV is the ^{8}Be α-separation energy, and E_R is the ^{8}Be recoil energy. The average recoil energy as a function of E_x determined from the decay generator was used to calculate E_R in a manner similar to that used in Ref. [23]. At 3-MeV excitation energy, the average recoil energy is about 7 keV and toward the Q value it approaches 0.

To determine uncertainties and extrapolate to low E_x, the FSD was fit using the standard R-matrix formulation [43] with channel radius at 4.5 fm [44]. Each 2^{+} state fed from

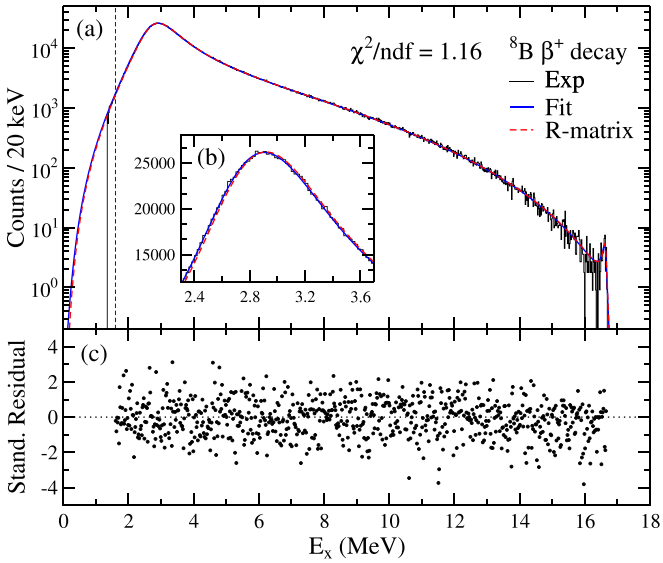

FIG. 1. ^{8}Be FSD from ^{8}B β^+ decay. The experimental data (black histogram) fit with our R-matrix prescription folded with the DSSD line shape (blue solid curve) are shown in panel (a). The corresponding unfolded R matrix is the red dashed curve. Panel (b) highlights the peak region. The vertical dotted line represents the 1.6-MeV low-energy bound for the fit. Panel (c) provides the standardized residuals for the fit.

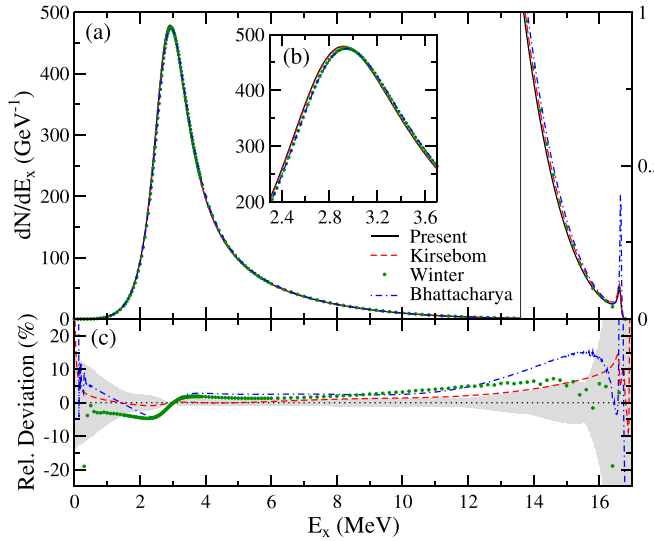

FIG. 2. Panel (a) shows the present FSD (black solid curve) compared to Kirsebom *et al.* [23] (red dashed curve), Winter *et al.* [21] (green dots), and Bhattacharya *et al.* [22] (blue dot-dashed curve). Panel (b) highlights the peak region. Panel (c) shows the relative deviations (FSD − FSD$_{\text{present}}$)/FSD$_{\text{present}}$. The gray band represents the 1σ uncertainty for the present FSD.

^{8}B β^+ decay was represented by its energy, reduced width, and decay strength in terms of Fermi and Gamow-Teller matrix elements. The first 2^+ state at 3 MeV has negligible Fermi strength [45,46]; its energy, width, and Gamow-Teller strength were free parameters.

The 16.626- and 16.922-MeV doublet states were treated as linear combinations of $T = 0$ and $T = 1$ isospin states [47] with decay strengths as described in, e.g., Refs. [21,23]. In Bhattacharya *et al.* [22], the doublet energies were fixed to 16.626 and 16.922 MeV and the doublet widths were fixed to the values of Ref. [48]. Likewise, Winter *et al.* [21] used the same energies and nearly identical widths. In Kirsebom *et al.* [23] and Roger *et al.* [24], Barker's parameter K, which was introduced to account for the interference of the narrow doublet states with other broad 2^+ levels [47,49,50], was incorporated. Here, in order to best describe the experimental data, the $K = 0$ values for the energies and widths of the doublet levels were taken from Refs. [48,51] and K was varied. Using a 4.5-fm channel radius, the best fit required $K = 0.8$, which corresponds to a nonresonant background-scattering phase shift of 60° and is lower than the $K = 1.3$ and 1.8 calculated using scattering phase shifts of 74° [47] and 82° [49,52], respectively. However, varying K from 0 to 2 changed the FSD fit χ^2 by less than 2%.

A fourth 2^+ state fixed at 37 MeV was included to account for background from β^+ decay to higher-lying levels. The width and the Gamow-Teller strength for this state were varied in the fit while the Fermi strength was fixed to 0 [21,23]. The R matrix was folded with the DSSD line-shape model and the spectrum was fit from 1.6 MeV to the Q value, 16.9578 MeV. The lower bound of the fit was chosen utilizing the decay generator, GEANT4 simulation, and sortcode and allowed a known input FSD to be reconstructed. This avoids the lower-energy region where the α and β distributions overlap and $\alpha-\beta$ coincidences could be mistaken as $\alpha-\alpha$ doubles.

The FSD uncertainties were evaluated using an empirical approach following Ref. [23]. The statistical uncertainty was taken as the standard error of the R-matrix fit parameters accounting for covariances. Systematic uncertainties were found by varying a fit aspect and taking the larger of the two differences from the original fit, $|\text{FSD}_{\pm}(E_x) - \text{FSD}(E_x)|$, as the symmetric uncertainty. For instance, the experimental α energies were shifted up and down by the 1σ calibration uncertainty. The resulting FSD spectra were fit with the above R-matrix model to produce $\text{FSD}_{\pm}(E_x)$. For the DSSD response systematic uncertainty, the incomplete charge collection fraction in the line-shape model was varied to 4 and 12% from 8%. Finally, the R-matrix model systematic uncertainty was determined by varying the channel radius and the background 2^+ level energy. For the first fit, the channel radius was set to 4.0 fm and the energy of the background 2^+ level was floated. For the other fit, the background level was treated as the "intruder" state within the β-decay Q value and allowed to vary from 7 to 13 MeV, necessitating the use of a larger, 6.7-fm channel radius [23,50].

The present FSD is broadly consistent with previous measurements with relative differences of around 5% at E_x from 0.5 MeV up to 14 MeV (see Fig. 2). At low E_x and near the doublet, there are bigger differences but larger uncertainties. The present FSD maximum is 2918(8) keV, consistent with the IGISOL result of 2921(5) keV [23] and the updated KVI result of 2923(6) keV [26] and in tension with the Winter *et al.* value of 2943(9) keV [21] and the Bhattacharya *et al.* value of 2939(5) keV [22] (see Fig. 3). Consequently, this work

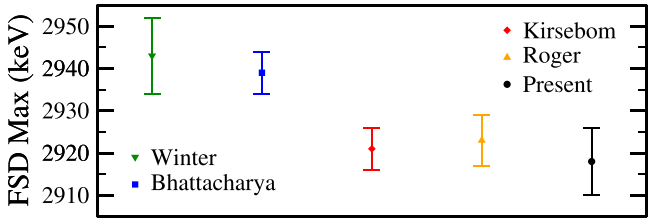

FIG. 3. The present FSD maximum (black circle) agrees with Kirsebom *et al.* [23] (red diamond) and Roger *et al.* [24,26] (yellow upward triangle) rather than Winter *et al.* [21] (green downward triangle) and Bhattacharya *et al.* [22] (blue square).

provides the first independent confirmation of the maximum suggested by the IGISOL/KVI collaboration. The present R-matrix fit parameters and the FSD with uncertainties are provided as Supplemental Material [53].

The neutrino energy spectrum was calculated from the present FSD following the method outlined by Winter *et al.* [21] and is obtained from

$$\frac{dN}{dE_\nu} \sim p_\beta E_\nu^2 (E_0 - E_x - E_\nu) F(-Z, E_\beta) R(E_\nu, E_0) C(E_\nu, E_0), \tag{1}$$

where p_β and E_β are the β^+ momentum and energy, E_ν is the neutrino energy, E_x is the ^{8}Be excitation energy, and the maximum β^+ energy accounting for the ^{8}Be recoil is $E_0 = Q + m_e - E_R$. The Fermi function $F(-Z, E_\beta)$ was taken from Ref. [54] and the radiative correction $R(E_\nu, E_0)$ was taken from Ref. [55]. The recoil-order correction $C(E_\nu, E_0)$ [38] depends on the terms b (weak magnetism), c (Gamow-Teller), d (induced tensor), and h (induced pseudoscalar). Following Ref. [21], b(E_x) was derived from the R-matrix fit parameters for ^{8}Be γ decay [56], while c(E_x) was derived from the present β^+ decay R-matrix fit parameters. The terms d(E_x) and h(E_x) were assumed to be proportional to c(E_x) [21]. At each neutrino energy from 0 to $Q - E_R(0)$, the neutrino spectrum value is calculated by integrating Eq. (1) weighted by FSD(E_x) over the allowed ^{8}Be excitation energies [0 to $Q - E_R(E_x) - E_\nu$]. The neutrino energy spectrum obtained is shown in Fig. 4.

The FSD uncertainties were propagated to the neutrino spectrum using the FSD$_\pm(E_x)$ curves described above to calculate neutrino spectra $F_\pm(E_\nu)$. For each uncertainty, the larger of the two differences $|F_\pm(E_\nu) - F(E_\nu)|$ was adopted as the corresponding symmetric uncertainty in the neutrino spectrum. The total uncertainty from the FSD uncertainties was evaluated by adding the individual sources in quadrature.

The recoil-order correction uncertainty is dominated by the uncertainty in b(E_x) from the radiative decay measurement [56]. The 1σ error bands on b(E_x) were calculated by propagating the uncertainties in the $M1$ γ-decay matrix elements for the 3-MeV state and doublet [56]. The systematic uncertainties on b(E_x) described in Ref. [21] (8% total) were also included. The recoil-order term b(E_x) was then varied up and down by the total 1σ error bands and the resulting uncertainty on the neutrino spectrum was taken from $|F_\pm(E_\nu) - F(E_\nu)|$. The width of the present uncertainty band due to the recoil-order correction uncertainty closely resembles the uncertainty band width in Fig. 12 of Ref. [21]. However, the shapes of the recoil-order corrections are slightly different since c(E_x) is not identical here and in Ref. [21]. The recoil-order uncertainty was added in quadrature with the FSD uncertainties to yield the total neutrino spectrum uncertainty.

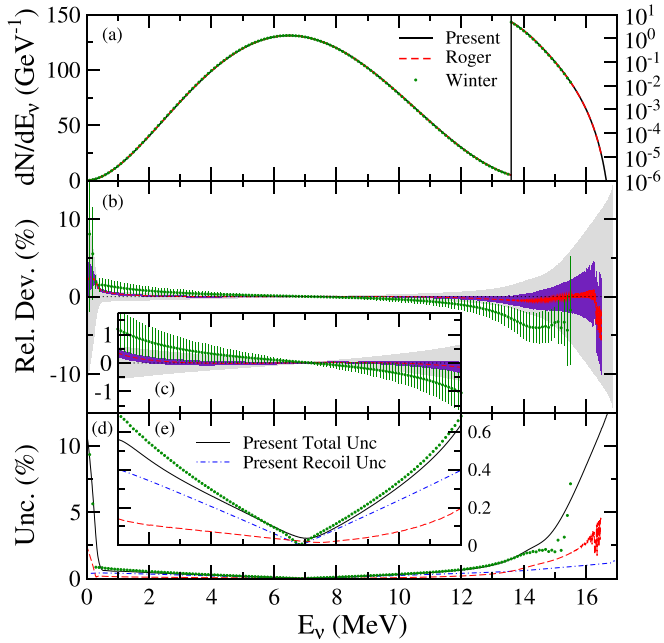

FIG. 4. Panel (a) compares the neutrino energy spectra $F(E_\nu)$ from the present work (black solid curve), Roger *et al.* [24] (red dashed curve), and Winter *et al.* [21] (green dots). Panel (b) shows the relative deviations $[F(E_\nu) - F(E_\nu)_{\text{present}}]/F(E_\nu)_{\text{present}}$. The present 1σ uncertainty band is light gray, while the 1σ uncertainty band for Ref. [24] is purple (dark gray). Panel (c) highlights the relative deviations over 1.5 to 12 MeV. Panel (d) shows the comparison of the present total uncertainty (black solid curve), the present uncertainty due to the recoil-order correction (blue dot-dashed curve), the uncertainty reported by Roger *et al.* [24] (red dashed curve), and the uncertainty reported by Winter *et al.* [21] (green dots). Panel (e) highlights the uncertainties over 1.5 to 12 MeV.

Figure 4 shows excellent agreement between the present neutrino energy spectrum and the spectrum from Roger *et al.*, which combines the IGISOL and KVI results [24]. The present neutrino spectrum with uncertainties is provided as Supplemental Material [53]. Between 1 and 12 MeV, the deviations with Ref. [24] are smaller than about 0.3%. Compared to the Winter spectrum, the deviations in this energy range are within roughly 1%. At higher energies, the deviations relative to Ref. [21] reach over 4% but mostly overlap within mutual uncertainties. Due to the $E_x = 1.6$ MeV lower limit in the R-matrix fit, the present neutrino spectrum is derived solely from extrapolation above about $E_\nu = 15.4$ MeV. Unlike in Refs. [23,24] and the present work, Winter *et al.* [21] did not consider an R-matrix model introducing an "intruder" 2^+ or allow the background 2^+ energy to vary. The choice of R-matrix model provides the largest contribution to the total uncertainty at low and high E_ν. Except at low and high E_ν, the uncertainty from Ref. [24] is smaller than the

uncertainty due to the recoil-order correction only, which is dominated by uncertainties from Ref. [56]. In Ref. [24], the recoil-order correction uncertainty was handled differently than in the present work and Ref. [21], possibly underestimating it. Higher-statistics measurements of the radiative decay of the doublet states similar to Ref. [56] and complementary measurements of b(E_x) (see, e.g., Ref. [57]) may be worthwhile. Furthermore, calculations of the recoil-order terms for ^{8}B β^+ decay similar to those for ^{8}Li β^- decay [58] should be performed to determine their impact on the recoil-order correction and its uncertainty.

In summary, the BPT was used to suspend ^{8}B ions in vacuum, yielding a new determination of the emitted neutrino spectrum. The ^{8}Be FSD maximum is 2918(8) keV, supporting the results of the IGISOL/KVI collaboration [23,24] rather than those of Refs. [21,22]. The neutrino spectrum calculated here agrees well with the combined IGISOL/KVI result [24]. Overall, this work distinguishes between the previous discrepant results for the neutrino energy spectrum from ^{8}B β^+ decay, providing a firm input with appropriate uncertainties for solar neutrino experiments, especially at next-generation facilities aiming to precisely measure neutrinos above 10 MeV to determine the 1–3% day/night effect and the *hep* neutrino flux [16].

This work was carried out under the auspices of the U.S. Department of Energy, by Argonne National Laboratory under Contract No. DE-AC02-06CH11357 and Lawrence Livermore National Laboratory under Contract No. DE-AC52-07NA27344. Funding by NSERC (Canada) under Contract No. SAPPJ-2018-0028 and the National Science Foundation under Grant No. PHY-2011890 is acknowledged. L.V. was supported by a National Science Foundation Graduate Research Fellowship under Grant No. DGE-1746045. This research used resources of Argonne National Laboratory's ATLAS facility, which is a DOE Office of Science User Facility. The authors thank G. D. Orebi Gann for discussions on solar neutrino experiments and T. Roger for providing the neutrino energy spectrum from Ref. [24].

[1] B. T. Cleveland, T. Daily, R. Davis, Jr., J. R. Distel, K. Lande, C. K. Lee, P. S. Wildenhain, and J. Ullman, Astrophys. J. **496**, 505 (1998).
[2] L. Wolfenstein, Phys. Rev. D **17**, 2369 (1978).
[3] S. P. Mikheyev and A. Y. Smirnov, Sov. J. Nucl. Phys. **42**, 913 (1985).
[4] H. A. Bethe, Phys. Rev. Lett. **56**, 1305 (1986).
[5] S. Fukuda, Y. Fukuda, M. Ishitsuka, Y. Itow, T. Kajita, J. Kameda, K. Kaneyuki, K. Kobayashi, Y. Koshio, M. Miura, S. Moriyama, M. Nakahata, S. Nakayama, A. Okada, N. Sakurai, M. Shiozawa, Y. Suzuki, H. Takeuchi, Y. Takeuchi, T. Toshito *et al.* (Super-Kamiokande Collaboration), Phys. Rev. Lett. **86**, 5651 (2001).
[6] Q. R. Ahmad, R. C. Allen, T. C. Andersen, J. D. Anglin, G. Bühler, J. C. Barton, E. W. Beier, M. Bercovitch, J. Bigu, S. Biller, R. A. Black, I. Blevis, R. J. Boardman, J. Boger, E. Bonvin, M. G. Boulay, M. G. Bowler, T. J. Bowles, S. J. Brice, M. C. Browne *et al.* (SNO Collaboration), Phys. Rev. Lett. **87**, 071301 (2001).
[7] Q. R. Ahmad, R. C. Allen, T. C. Andersen, J. D.Anglin, J. C. Barton, E. W. Beier, M. Bercovitch, J. Bigu, S. D. Biller, R. A. Black, I. Blevis, R. J. Boardman, J. Boger, E. Bonvin, M. G. Boulay, M. G. Bowler, T. J. Bowles, S. J. Brice, M. C. Browne, T. V. Bullard *et al.* (SNO Collaboration), Phys. Rev. Lett. **89**, 011301 (2002).
[8] M. Agostini, K. Altenmüller, S. Appel, V. Atroshchenko, Z. Bagdasarian, D. Basilico, G. Bellini, J. Benziger, D. Bick, G. Bonfini, D. Bravo, B. Caccianiga, F. Calaprice, A. Caminata, S. Caprioli, M. Carlini, P. Cavalcante, A. Chepurnov, K. Choi, L. Collica *et al.* (Borexino Collaboration), Nature (London) **562**, 505 (2018).
[9] S. Abe, K. Furuno, A. Gando, Y. Gando, K. Ichimura, H. Ikeda, K. Inoue, Y. Kibe, W. Kimura, Y. Kishimoto, M. Koga, Y. Minekawa, T. Mitsui, T. Morikawa, N. Nagai, K. Nakajima, K. Nakamura, M. Nakamura, K. Narita, I. Shimizu *et al.* (KamLAND Collaboration), Phys. Rev. C **84**, 035804 (2011).
[10] K. Abe, Y. Haga, Y. Hayato, M. Ikeda, K. Iyogi, J. Kameda, Y. Kishimoto, L. Marti, M. Miura, S. Moriyama, M. Nakahata, T. Nakajima, S. Nakayama, A. Orii, H. Sekiya, M. Shiozawa, Y. Sonoda, A. Takeda, H. Tanaka, Y. Takenaga *et al.* (Super-Kamiokande Collaboration), Phys. Rev. D **94**, 052010 (2016).
[11] M. Anderson, S. Andringa, S. Asahi, M. Askins, D. J. Auty, N. Barros, D. Bartlett, F. Barão, R. Bayes, E. W. Beier, A. Bialek, S. D. Biller, E. Blucher, R. Bonventre, M. Boulay, E. Caden, E. J. Callaghan, J. Caravaca, D. Chauhan, M. Chen *et al.* (SNO+ Collaboration), Phys. Rev. D **99**, 012012 (2019).
[12] F. Capozzi, S. W. Li, G. Zhu, and J. F. Beacom, Phys. Rev. Lett. **123**, 131803 (2019).
[13] M. Agostini, K. Altenmüller, S. Appel, V. Atroshchenko, Z. Bagdasarian, D. Basilico, G. Bellini, J. Benziger, D. Bick, D. Bravo, B. Caccianiga, F. Calaprice, A. Caminata, P. Cavalcante, A. Chepurnov, D. D'Angelo, S. Davini, A. Derbin, A. Di Giacinto, V. Di Marcello *et al.* (Borexino Collaboration), Phys. Rev. D **101**, 062001 (2020).
[14] I. Lopes and J. Silk, Phys. Rev. D **99**, 023008 (2019).
[15] W. Ma, A. Abdukerim, C. Cheng, Z. Bo, W. Chen, X. Chen, Y. Chen, Z. Cheng, X. Cui, Y. Fan, D. Fang, C. Fu, M. Fu, L. Geng, K. Giboni, L. Gu, X. Guo, C. Han, K. Han, C. He *et al.* (PandaX Collaboration), Phys. Rev. Lett. **130**, 021802 (2023).
[16] G. D. Orebi Gann, K. Zuber, D. Bemmerer, and A. Serenelli, Annu. Rev. Nucl. Part. Sci. **71**, 491 (2021).
[17] J. N. Bahcall, E. Lisi, D. E. Alburger, L. De Braeckeleer, S. J. Freedman, and J. Napolitano, Phys. Rev. C **54**, 411 (1996).
[18] C. E. Ortiz, A. García, R. A. Waltz, M. Bhattacharya, and A. K. Komives, Phys. Rev. Lett. **85**, 2909 (2000).
[19] E. G. Adelberger, A. García, R. G. H. Robertson, K. A. Snover, A. B. Balantekin, K. Heeger, M. J. Ramsey-Musolf, D. Bemmerer, A. Junghans, C. A. Bertulani, J.-W. Chen, H. Costantini, P. Prati, M. Couder, E. Uberseder, M. Wiescher, R. Cyburt, B. Davids, S. J. Freedman, M. Gai *et al.*, Rev. Mod. Phys. **83**, 195 (2011).
[20] W. T. Winter, S. J. Freedman, K. E. Rehm, I. Ahmad, J. P. Greene, A. Heinz, D. Henderson, R. V. F. Janssens, C. L. Jiang, E. F. Moore, G. Mukherjee, R. C. Pardo, T. Pennington, G. Savard, J. P. Schiffer, D. Seweryniak, G. Zinkann, and M. Paul, Phys. Rev. Lett. **91**, 252501 (2003).

[21] W. T. Winter, S. J. Freedman, K. E. Rehm, and J. P. Schiffer, Phys. Rev. C **73**, 025503 (2006).

[22] M. Bhattacharya, E. G. Adelberger, and H. E. Swanson, Phys. Rev. C **73**, 055802 (2006).

[23] O. S. Kirsebom, S. Hyldegaard, M. Alcorta, M. J. G. Borge, J. Büscher, T. Eronen, S. Fox, B. R. Fulton, H. O. U. Fynbo, H. Hultgren, A. Jokinen, B. Jonson, A. Kankainen, P. Karvonen, T. Kessler, A. Laird, M. Madurga, I. Moore, G. Nyman, H. Penttilä *et al.*, Phys. Rev. C **83**, 065802 (2011).

[24] T. Roger, J. Büscher, B. Bastin, O. S. Kirsebom, R. Raabe, M. Alcorta, J. Äystö, M. J. G. Borge, M. Carmona-Gallardo, T. E. Cocolios, J. Cruz, P. Dendooven, L. M. Fraile, H. O. U. Fynbo, D. Galaviz, L. R. Gasques, G. S. Giri, M. Huyse, S. Hyldegaard, K. Jungmann *et al.*, Phys. Rev. Lett. **108**, 162502 (2012).

[25] S. J. Freedman, K. E. Rehm, J. P. Schiffer, and D. Seweryniak, Phys. Rev. Lett. **109**, 189201 (2012).

[26] T. Roger, O. S. Kirsebom, H. O. U. Fynbo, and R. Raabe, Phys. Rev. Lett. **109**, 189202 (2012).

[27] O. S. Kirsebom, H. O. U. Fynbo, K. Riisager, R. Raabe, and T. Roger, Nucl. Instrum. Methods Phys. Res., Sect. A **758**, 57 (2014).

[28] N. D. Scielzo, G. Li, M. G. Sternberg, G. Savard, P. F. Bertone, F. Buchinger, S. Caldwell, J. A. Clark, J. Crawford, C. M. Deibel, J. Fallis, J. P. Greene, S. Gulick, A. A. Hecht, D. Lascar, J. K. P. Lee, A. F. Levand, M. Pedretti, R. E. Segel, H. Sharma *et al.*, Nucl. Instrum. Methods Phys. Res., Sect. A **681**, 94 (2012).

[29] G. Li, R. Segel, N. D. Scielzo, P. F. Bertone, F. Buchinger, S. Caldwell, A. Chaudhuri, J. A. Clark, J. E. Crawford, C. M. Deibel, J. Fallis, S. Gulick, G. Gwinner, D. Lascar, A. F. Levand, M. Pedretti, G. Savard, K. S. Sharma, M. G. Sternberg, T. Sun *et al.*, Phys. Rev. Lett. **110**, 092502 (2013).

[30] M. G. Sternberg, R. Segel, N. D. Scielzo, G. Savard, J. A. Clark, P. F. Bertone, F. Buchinger, M. Burkey, S. Caldwell, A. Chaudhuri, J. E. Crawford, C. M. Deibel, J. Greene, S. Gulick, D. Lascar, A. F. Levand, G. Li, A. Pérez Galván, K. S. Sharma, J. Van Schelt *et al.*, Phys. Rev. Lett. **115**, 182501 (2015).

[31] M. T. Burkey, G. Savard, A. T. Gallant, N. D. Scielzo, J. A. Clark, T. Y. Hirsh, L. Varriano, G. H. Sargsyan, K. D. Launey, M. Brodeur, D. P. Burdette, E. Heckmaier, K. Joerres, J. W. Klimes, K. Kolos, A. Laminack, K. G. Leach, A. F. Levand, B. Longfellow, B. Maaß *et al.*, Phys. Rev. Lett. **128**, 202502 (2022).

[32] T. Y. Hirsh, A. Pérez Gálvan, M. T. Burkey, A. Aprahamian, F. Buchinger, S. Caldwell, J. A. Clark, A. T. Gallant, E. Heckmaier, A. F. Levand, S. T. Marley, G. E. Morgan, A. Nystrom, R. Orford, G. Savard, N. D. Scielzo, R. Segel, K. S. Sharma, K. Siegl, and B. S. Wang, Nucl. Instrum. Methods Phys. Res., Sect. A **887**, 122 (2018).

[33] J. Fallis, Ph.D. thesis, University of Manitoba, 2009.

[34] G. Savard, St. Becker, G. Bollen, H.-J. Kluge, R. B. Moore, Th. Otto, L. Schweikhard, H. Stolzenberg, and U. Wiess, Phys. Lett. A **158**, 247 (1991).

[35] Y. A. Akovali, Nucl. Data Sheets **84**, 1 (1998).

[36] B. Singh and E. Browne, Nucl. Data Sheets **109**, 2439 (2008).

[37] F. Glück, Nucl. Phys. A **628**, 493 (1998).

[38] B. R. Holstein, Rev. Mod. Phys. **46**, 789 (1974).

[39] G. Bortels and P. Collaers, Appl. Radiat. Isot. **38**, 831 (1987).

[40] L. Reggiani and V. Mitin, Riv. Nuovo Cim. **12**, 1 (1989).

[41] E. Kamieniecki, J. Appl. Phys. **116**, 193702 (2014).

[42] D.-M. Mei, R. B. Mukund, W.-Z. Wei, R. Panth, J. Liu, H. Mei, Y.-Y. Li, P. Acharya, S. Bhattarai, K. Kooi, M.-S. Raut, X.-S. Sun, A. Kirkvold, K.-M. Dong, X.-H. Meng, G.-J. Wang, and G. Yang, J. Phys. G: Nucl. Part. Phys. **47**, 105106 (2020).

[43] A. M. Lane and R. G. Thomas, Rev. Mod. Phys. **30**, 257 (1958).

[44] E. K. Warburton, Phys. Rev. C **33**, 303 (1986).

[45] R. D. McKeown, G. T. Garvey, and C. A. Gagliardi, Phys. Rev. C **22**, 738 (1980).

[46] R. B. Wiringa, S. Pastore, S. C. Pieper, and G. A. Miller, Phys. Rev. C **88**, 044333 (2013).

[47] F. C. Barker, Aust. J. Phys. **22**, 293 (1969).

[48] F. Ajzenberg-Selove, Nucl. Phys. A **413**, 1 (1984).

[49] F. Hinterberger, P. D. Eversheim, P. Von Rossen, B. Schüller, R. Schönhagen, M. Thenée, R. Görgen, T. Braml, and H. J. Hartmann, Nucl. Phys. A **299**, 397 (1978).

[50] F. C. Barker, Aust. J. Phys. **42**, 25 (1989).

[51] D. R. Tilley, J. H. Kelley, J. L. Godwin, D. J. Millener, J. E. Purcell, C. G. Sheu, and H. R. Weller, Nucl. Phys. A **745**, 155 (2004).

[52] A. D. Bacher, F. G. Resmini, H. E. Conzett, R. de Swiniarski, H. Meiner, and J. Ernst, Phys. Rev. Lett. **29**, 1331 (1972).

[53] See Supplemental Material at http://link.aps.org/supplemental/10.1103/PhysRevC.107.L032801 for the present R-matrix fit parameters, FSD with uncertainties, and neutrino spectrum with uncertainties.

[54] H. Behrens and J. Jänecke, in *Numerical Tables for Beta-Decay and Electron Capture*, edited by H. Schopper (Springer-Verlag, Berlin, 1969).

[55] A. Sirlin, Phys. Rev. D **84**, 014021 (2011).

[56] L. De Braeckeleer, E. G. Adelberger, J. H. Gundlach, M. Kaplan, D. Markoff, A. M. Nathan, W. Schieff, K. A. Snover, D. W. Storm, K. B. Swartz, D. Wright, and B. A. Brown, Phys. Rev. C **51**, 2778 (1995).

[57] T. Sumikama, K. Matsuta, T. Nagatomo, M. Ogura, T. Iwakoshi, Y. Nakashima, H. Fujiwara, M. Fukuda, M. Mihara, K. Minamisono, T. Yamaguchi, and T. Minamisono, Phys. Rev. C **83**, 065501 (2011).

[58] G. H. Sargsyan, K. D. Launey, M. T. Burkey, A. T. Gallant, N. D. Scielzo, G. Savard, A. Mercenne, T. Dytrych, D. Langr, L. Varriano, B. Longfellow, T. Y. Hirsh, and J. P. Draayer, Phys. Rev. Lett. **128**, 202503 (2022).